ECE 795:

Quantitative Electrophysiology

Notes for Lecture #4

Wednesday, October 4, 2006

7. CHEMICAL SYNAPSES AND GAP JUNCTIONS

We will look at:

- Chemical synapses in the nervous system
- Gap junctions in cardiac cells and nervous tissue

Chemical synapses:

The specialized contact zones between neurons are called *synapses*.

In the nervous system, *chemical synapses* are much more common than *electrical synapses* (*gap junctions*).

Most chemical synapses are unidirectional — the *presynaptic* neuron releases *neurotransmitter* across the *synaptic cleft* to the *postsynaptic terminal*, which leads to activation of a neurotransmitter-gated ion channel.

Chemical synapses (cont.):

In the electron micrograph below, a presynaptic body in the inner hair cell is seen to hold a cluster of neurotransmitter vesicles. A thickening of the cell membranes is observed between the pre- and post-synaptic terminals, and a very narrow synaptic cleft exists.

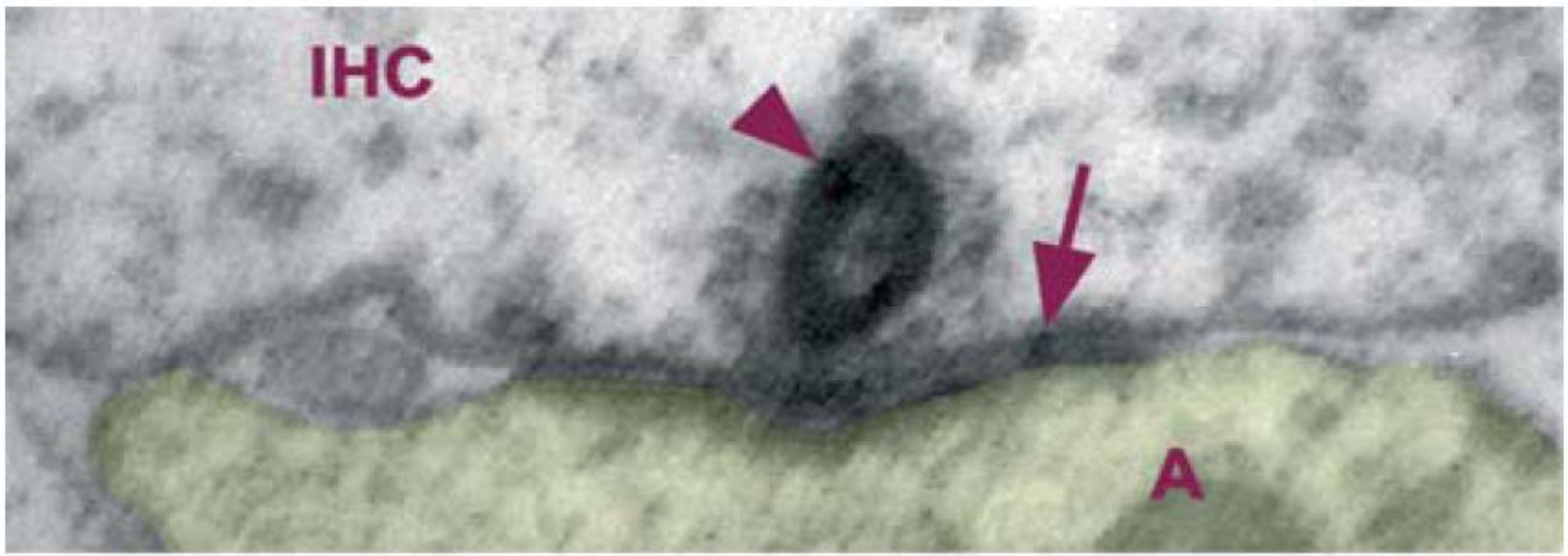

(from Francis et al., Brain Res. 2004)

Chemical synapses (cont.):

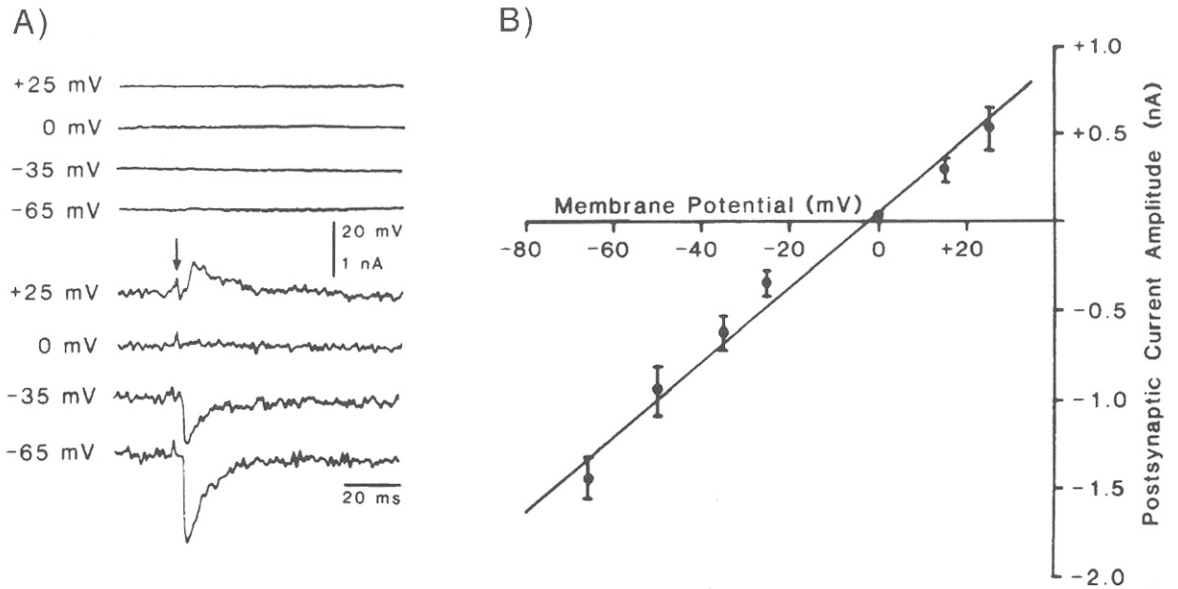

Fig. 1.6 A Fast Excitatory Synaptic Input Excitatory postsynaptic current (EPSC) caused by the simultaneous activation of synapses (arrow) made by the mossy fibers onto CA3 pyramidal cells in the rodent hippocampus (Brown and Johnston, 1983). This classical experiment showed how a central synapse can be successfully voltage clamped. **(A)** The voltage-clamp setup stabilizes—via electronic feedback control—the membrane potential at a fixed value. Here four experiments are shown, carried out at the holding potentials indicated at the left. The current that is drawn to keep the membrane potential constant, termed the clamp current, corresponds to the negative EPSC. It is maximal at negative potentials and reverses sign around zero. The synaptic current rises within 1 msec to its peak value, decaying to baseline over 20–30 msec. The experiments were carried out in the presence of pharmacological agents that blocked synaptic inhibition. **(B)** When the peak EPSC is plotted against the holding potential, an approximately linear relationship emerges; the regression line yields an x-axis intercept of -1.9 mV and a slope of 20.6 nS. Thus, once the synaptic reversal potential is accounted for, Ohm's law appears to be reasonably well obeyed. We conclude that synaptic input is caused by a transient increase in the conductance of the membrane to certain ions. Reprinted by permission from Brown and Johnston (1983).

(from Koch)

Chemical synapses (cont.):

Equivalent electric circuit of a fast chemical synapse:

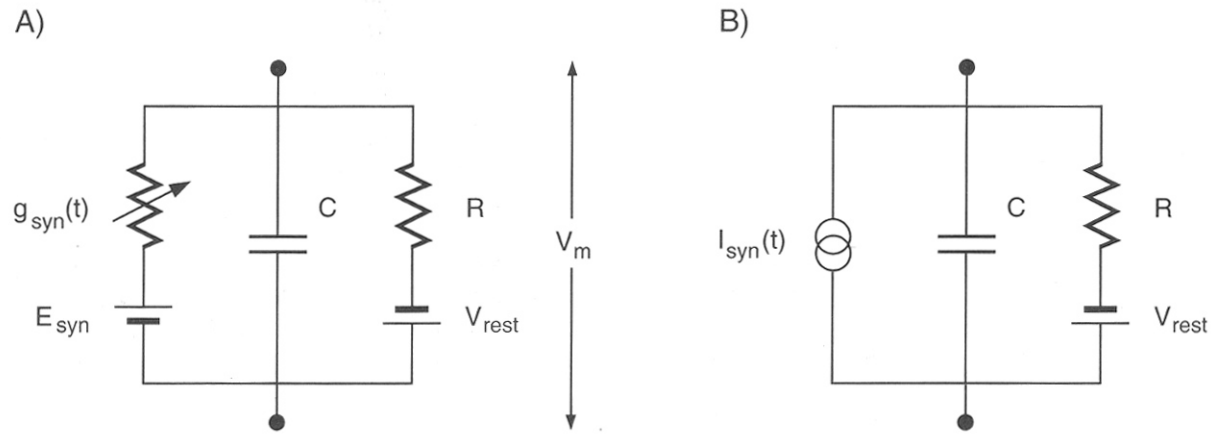

Fig. 1.7 Equivalent Electrical Circuit of a Fast Chemical Synapse **(A)** Electrical model of a fast voltage-independent chemical synapse. This circuit was put forth to explain events occurring at the neuromuscular junction by Katz (1969). Remarkably, all fast chemical synapses in the central nervous system, with the exception of the voltage-dependent NMDA receptor-synaptic complex, operate on the same principle. Activation of the synapse leads to the transient opening of ionic channels, selective to certain ions. This corresponds to a transient increase in the membrane conductance $g_{syn}(t)$ in series with the synaptic reversal potential E_{syn}, shown here in parallel with a passive membrane patch. **(B)** If the evoked potential change is small relative to the synaptic reversal potential, the synapse can be approximated by a current source of amplitude $g_{syn}(t)E_{syn}$. In general, however, this will not be the case and synaptic input must be treated as a conductance change, a fact that has important functional consequences.

(from Koch)

Chemical synapses (cont.):

The *postsynaptic current* (PSC) has the same form as a voltage-gated ion channel:

$$I_{\mathrm{syn}} = g_{\mathrm{syn}}(t)\,[V_m(t) - E_{\mathrm{syn}}]\,, \qquad \text{(K1.18)}$$

but the conductance $g_{\mathrm{syn}}(t)$ is controlled by the reception of neurotransmitter (rather than the transmembrane potential), which has a waveform that is often approximated by a so-called alpha function:

$$g_{\mathrm{syn}}(t) = \mathrm{const} \cdot t\, \mathrm{e}^{-t/t_{\mathrm{peak}}}. \qquad \text{(K1.21)}$$

Chemical synapses (cont.):

The direction of the postsynaptic current depends on the value of E_{syn}:

- if $E_{\text{syn}} > V_{\text{rest}}$, then I_{syn} will be a negative (i.e., inward) current, which will *depolarize* the cell.
  Consequently, this current is referred to as an *excitatory postsynaptic current* (EPSC), and the resulting membrane depolarization is referred to as an *excitatory postsynaptic potential* (EPSP).

Chemical synapses (cont.):

- if $E_{\text{syn}} < V_{\text{rest}}$, then I_{syn} will be a positive (i.e., outward) current, which will *hyperpolarize* the cell. Because hyperpolarization takes the membrane potential further away from the threshold potential, this is a form of *inhibition*. Consequently, this current is referred to as an *inhibitory postsynaptic current* (IPSC), and the resulting membrane hyperpolarization is referred to as an *inhibitory postsynaptic potential* (IPSP).

Chemical synapses (cont.):

- if $E_{\mathrm{syn}} \approx V_{\mathrm{rest}}$, then I_{syn} will be a negligible when the membrane is at rest. However, if current is injected into the membrane by a propagating EPSP or action potential or an applied current source, the increased conductance of $g_{\mathrm{syn}}(t)$ will tend to "shunt" this injected current, such that the membrane is locked at V_{rest}. Because this prevents action potential generation, it is referred to as *shunting inhibition*.

Chemical synapses (cont.):

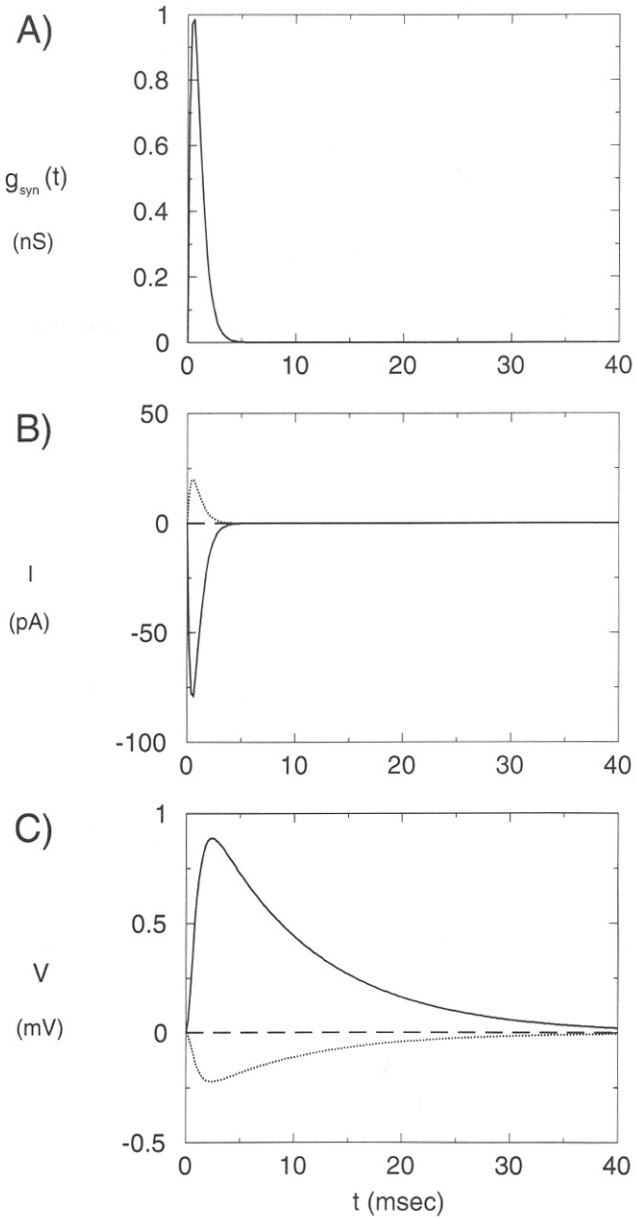

Fig. 1.8 Action of a Single Synapse Inserted into a Membrane Three different types of synaptic inputs and their differential effect on the membrane potential. **(A)** Time course of the synaptic-induced conductance increase, here with t_{peak}=0.5 msec and g_{peak} = 1 nS (Eq. 1.21). The synapse is inserted into a patch of membrane (Fig. 1.7A) with R = 100 MΩ, C = 100 pF, and τ = 10 msec. **(B)** Postsynaptic current in response to the conductance increase if the synaptic reversal potential is positive (E_{syn} = 80 mV relative to rest; solid line), negative (E_{syn} = −20 mV; dotted line), and zero (so-called shunting inhibition; dashed line). By convention, an inward current that depolarizes the cell is plotted as a negative current. **(C)** Associated EPSP (solid line) and IPSP (lower dashed line), relative to V_{rest}, solved by numerical integration of Eq. 1.20. Notice that the time course of the postsynaptic potential is much longer than the time course of the corresponding postsynaptic current due to the low-pass nature of the membrane. Shunting inhibition by itself does not give rise to any change in potential (center dashed line).

(from Koch)

Chemical synapses (cont.):

Shunting inhibition is most effective if placed on the path between an excitatory synapse and the soma.

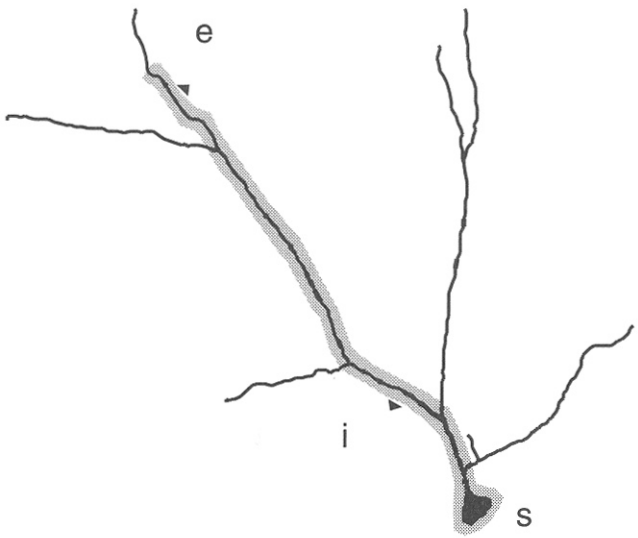

(from Koch)

Fig. 5.2 Interaction among an Excitatory and an Inhibitory Synapse How does the interaction between an excitatory synapse (at location *e*) and an inhibitory synapse (at *i*) in a passive dendritic tree depend on their spatial positions? And what role do the synaptic architecture and the dendritic morphology play? In general, the potential at the soma *s* is not simply the sum of the individual IPSP and EPSP but can be much less. If the inhibition is of the *shunting* type, with a reversal potential close to the resting potential of the cell, inhibition by itself leads to no significant potential change while still being able to veto the EPSP, as long as the inhibitory synapse is either close to the excitatory one or "on the direct path" between excitation and the soma *s* (shaded area). The effectiveness of shunting inhibition drops substantially outside this zone.

Gap junctions in cardiac cells:

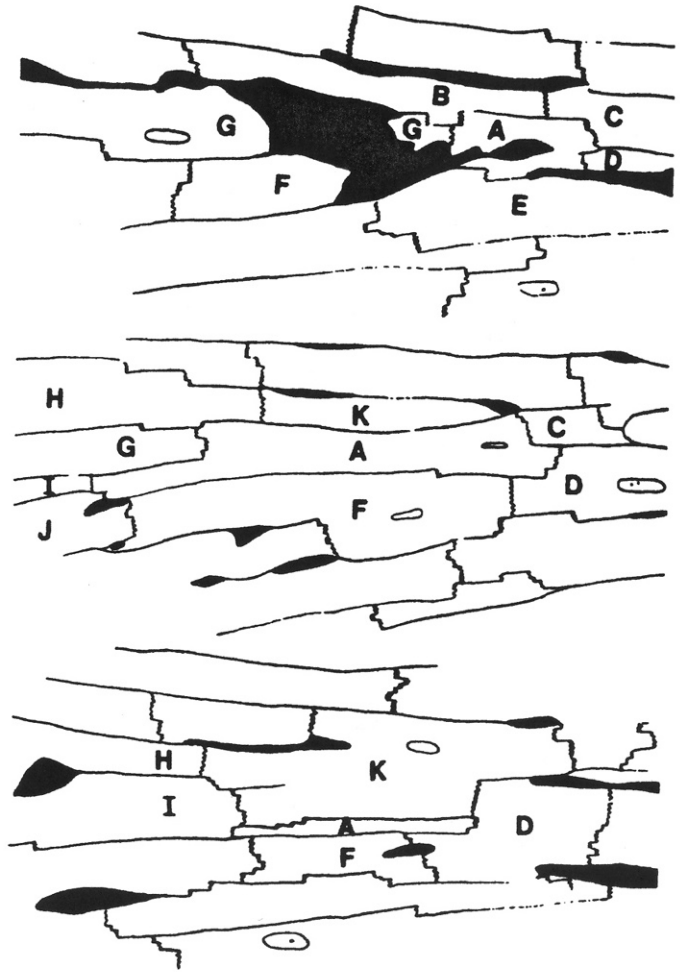

Figure 9.3. Structure of cardiac muscle. The figure shows three camera lucida drawings from a series of 42 consecutive 2-μm-thick plastic sections showing multiplicity of interconnections of the myocytes at intercalated disks. Shaded areas denote prominent interstitial vessels and septae. From top to bottom are shown sections 12, 16, and 22. Myocyte A is followed in its entirety and makes contact at intercalated discs with cells B–K. [R. H. Hoyt, M. L. Cohen, and J. E. Saffitz, Distribution and three-dimensional structure of the intercellular junctions in canine myocardium, *Circ. Res.* **64**:563–574 (1989).]

Gap junctions in cardiac cells (cont.):

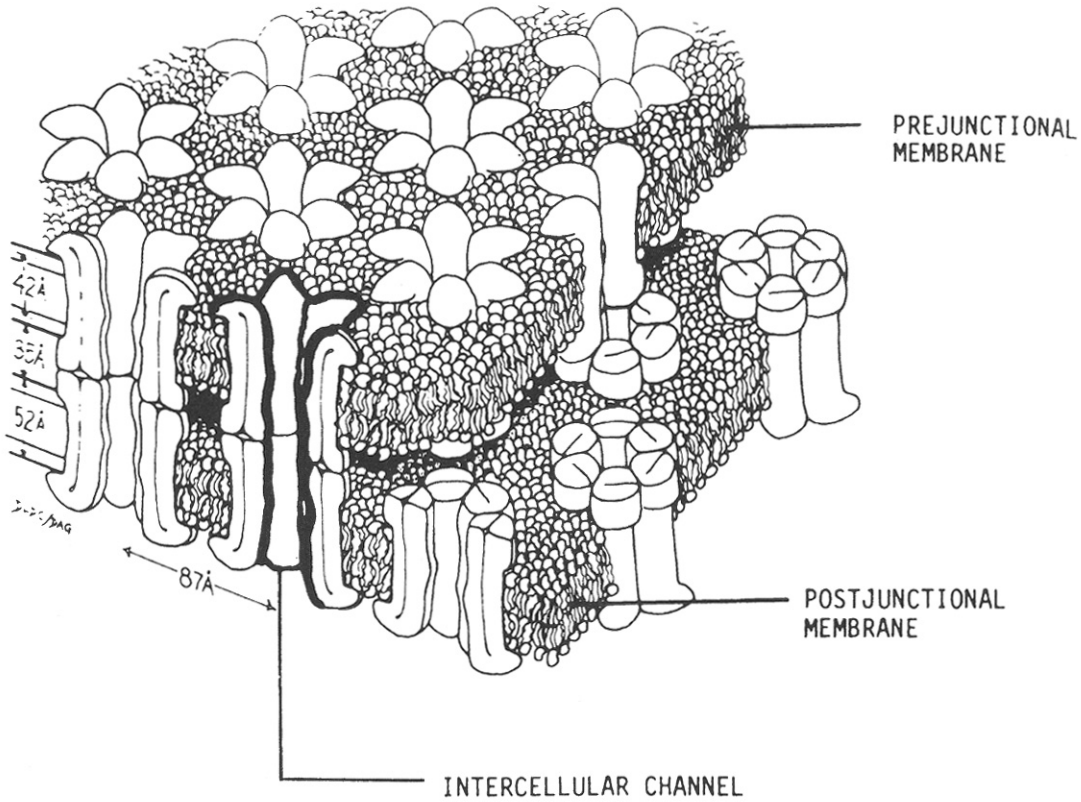

Figure 9.4. Details of the communicating-type intercellular cardiac junction (connexon array) is shown. Each unit (connexon) is a protein channel running transverse to the opposing membranes. Connexons from abutting cells align themselves to form structural continuity. The structural detail shown is based on morphometry obtained from X-ray diffraction, electron microscopy, and chemical studies. The gap spacing is given as 35 Å. [R. Plonsey, The use of a bidomain model for the study of excitable media, *Lectures on Mathematics in the Life Sciences* **21**:123–149 (1989). From L. Makowski, D. L. D. Caspar, W.C. Phillips, and D. A. Goodenough, Gap junctional structures II. Analysis of x-ray diffraction, *J. Cell Biol.* **74**:629–645 (1977). Reproduced from the Journal of Cell Biology, 1977, vol. 74, pp. 629–645 by copyright permission of the Rockefeller University Press.]

Gap junctions in cardiac cells (cont.):

Cable analysis of Purkinje fibers gives $\lambda \approx 1\ \mathrm{mm}$ and $\tau = 18\ \mathrm{ms}$.

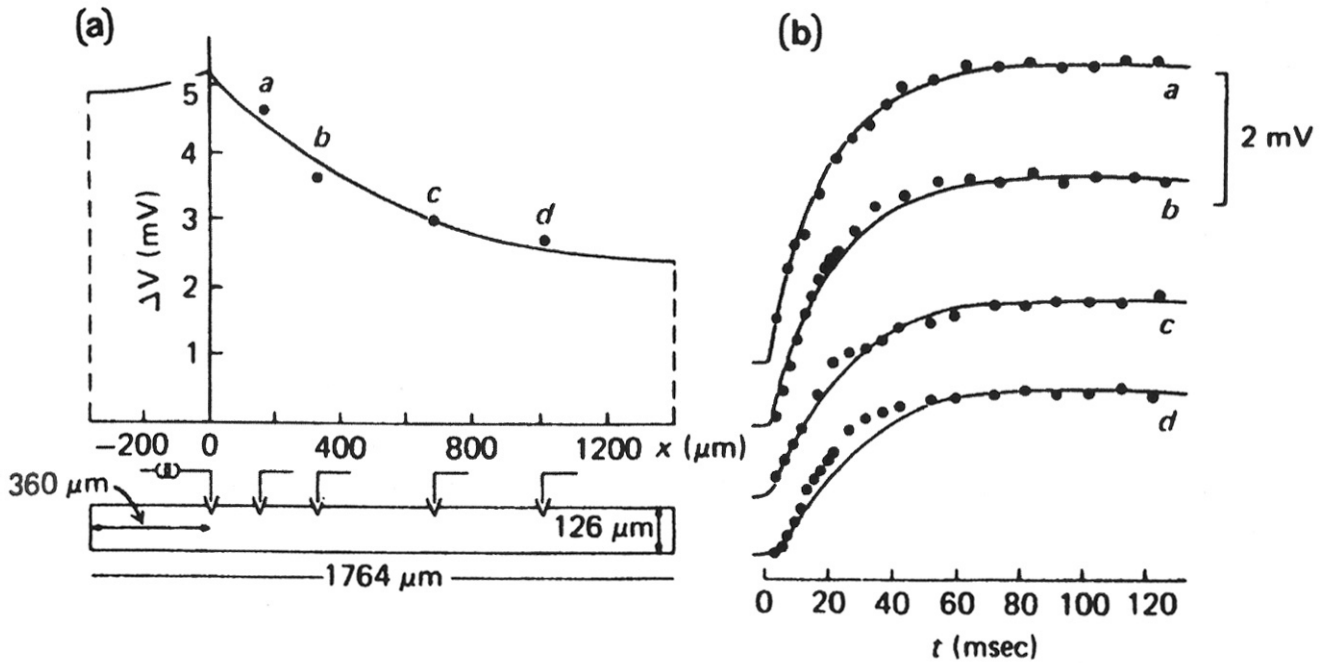

Figure 9.5. Cable analysis of rabbit Purkinje fiber. (a) Steady-state electrotonic response to an applied current step. Inset shows fiber geometry and the location of the current passing and voltage recording microelectrode impalement sites. (b) Temporal response at labeled sites. [From T. J. Colatsky and R. W. Tsien, Electrical properties associated with wide intercellular clefts in rabbit Purkinje fibers, *J. Physiol.* **290**:227–252 (1979)].

Gap junctions in cardiac cells (cont.):

Experimental estimation of gap junction resistance in dissociated cardiac cells.

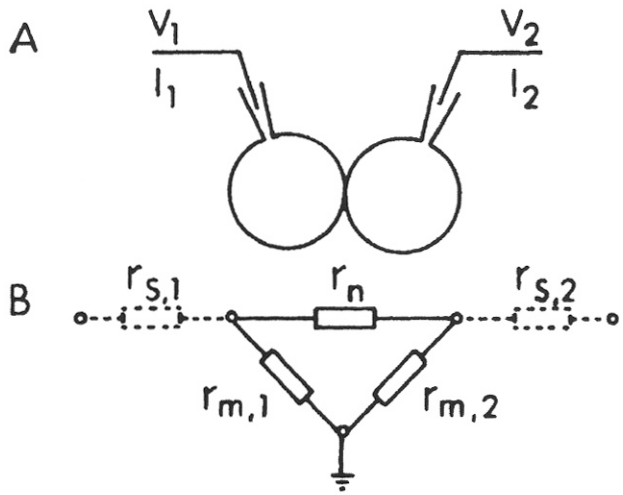

Figure 9.7. Diagram of the experimental arrangement. Each cell of a cell pair is connected to a voltage-clamp circuit via a patch electrode in the whole-cell configuration. Separate voltages V_1, V_2 can be applied to each cell and the resulting currents I_1, I_2 measured. (Subscripts 1, 2 refer to cells 1 and 2 as described in A.) The equivalent circuit is shown in B. The sarcolemmal resistance is denoted by r_{m1}, r_{m2}, the junctional (nexal) resistance by r_n, and the access (pipette) resistance, shown dotted, by r_{s1}, r_{s2}. [From R. Weingart, Electrical properties of the nexal membrane studied in rat ventricular pairs, *J. Physiol.* **370**:267–284 (1986).]

Gap junctions in cardiac cells (cont.):

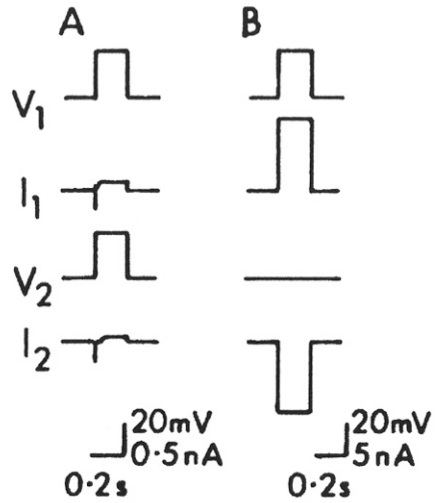

Figure 9.8. Current flow in a cardiac cell pair under voltage-clamp conditions. (A) Symmetrical pulse application ($V_1 = V_2 = 27$ mV applied for 200 ms). The associated current signals I_1 and I_2 show a time-dependent inward component; this reflects a sarcolemmal current only. (B) asymmetrical pulse application [$V_1 = 27$ mV for 200 ms; as in (A), $V_2 = 0$]. The signals I_1 and I_2 now show large amplitudes and no time-dependency. [Note the tenfold increase in scale compared to (A).] The holding potential $V_H = -42$ mV in (A) and (B). [From R. Weingart, Electrical properties of the nexal membrane studied in rat ventricular pairs, *J. Physiol.* **370**:267–284 (1986).]

$$\Rightarrow r_n = 1.7\ \mathrm{M}\Omega\,. \qquad (9.6)$$

Gap junctions in cardiac cells (cont.):

Estimation of gap junction resistance in chick embryo cell pairs.

$$\Rightarrow$$

$$r_n = 0.13\ \mathrm{M}\Omega\,. \qquad (9.8)$$

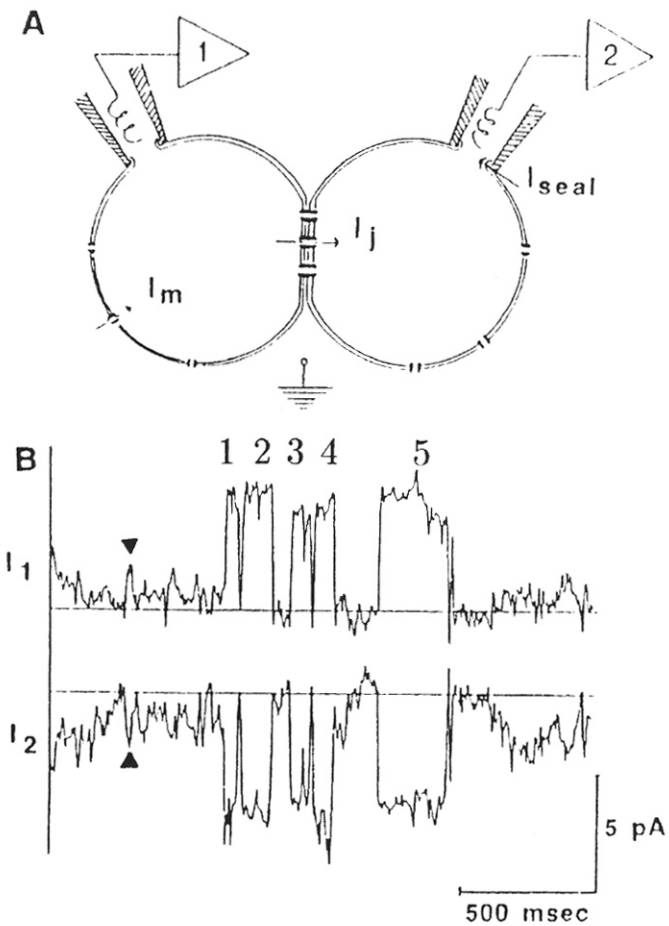

Figure 9.9. Two-cell preparation with $V_1 = -40$ mV, $V_2 = -80$ mV. The sarcoplasmic currents were measured separately by applying equal values of V_1 and V_2 and subtracted from the total current with the above values of V_1 and V_2 leaving only the junctional current $I_j = \pm(V_2 - V_1)/r_n$. The five distinct quantal events (numbered) are assumed to result from single channel openings. [From R. D. Veenstra and R. L. De Haan, Measurements of single channel currents from cardiac gap junctions, *Science* **233**:972–974 (1986). Copyright 1986 American Association for the Advancement of Science.]

Gap junctions in nervous tissue:

Gap junctions are found between :-

- some neurons, mainly during development,
- glial cells, and
- glial cells & neurons.

For more details, see:

Brain Research Reviews **32**(1), 2000.

8. DENDRITIC TREES

We will look at:

- Properties of infinite, semi-infinite & finite cables
- Branching in passive dendritic trees
- Equivalent cylinder of a dendritic tree
- Compartmental modeling

Dendritic tree morphology:

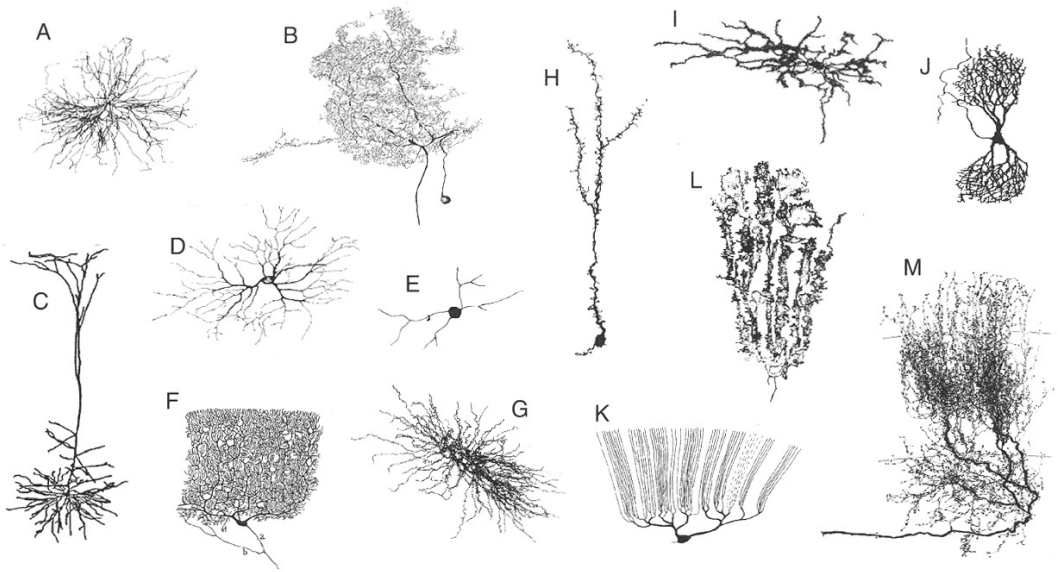

Fig. 3.1 DENDRITIC TREES OF THE WORLD Great variety of dendritic trees (in addition to a glia cell and an axonal tree) observed in the nervous systems of animals. The cells are not drawn to scale. **(A)** α motoneuron in spinal cord of cat (2.6 mm). Reprinted by permission from Cullheim, Fleshman, and Burke (1987). **(B)** Spiking interneuron in mesothoracic ganglion of locust (0.54 mm). Unpublished data from G. Laurent, with permission. **(C)** Layer 5 neocortical pyramidal cell in rat (1.03 mm). Reprinted by permission from Amitai et al., (1993). **(D)** Retinal ganglion cell in postnatal cat (0.39 mm). Reprinted by permission from Maslim, Webster, and Stone (1986). **(E)** Amacrine cell in retina of larval tiger salamander (0.16 mm). Reprinted by permission from Yang and Yazulla (1986). **(F)** Cerebellar Purkinje cell in human. Reprinted by permission from Ramón y Cajal (1909). **(G)** Relay neuron in rat ventrobasal thalamus (0.35 mm). Reprinted by permission from Harris (1986). **(H)** Granule cell from olfactory bulb of mouse (0.26 mm). Reprinted by permission from Greer (1987). **(I)** Spiny projection neuron in rat striatum (0.37 mm). Reprinted by permission from Penny, Wilson, and Kitai (1988). **(J)** Nerve cell in the nucleus of Burdach in human fetus. Reprinted by permission from Ramón y Cajal (1909). **(K)** Purkinje cell in mormyrid fish (0.42 mm). Reprinted by permission from Meek and Nieuwenhuys (1991). **(L)** Golgi epithelial (glia) cell in cerebellum of normal-reeler mouse chimera (0.15 mm). Reprinted by permission from Terashima et al., (1986). **(M)** Axonal arborization of isthmotectal neurons in turtle (0.46 mm). Reprinted by permission from Sereno and Ulinski (1987). The lengths given are approximate and correspond to the maximal extent. Reprinted by permission from Mel (1994).

(from Koch)

Steady-state response of a finite cable:

The steady-state response of a cable of finite length l in absolute units (or $L = l/\lambda$ in *electrotonic units*) can be described by one of the equivalent forms:

$$V(X) = A_1 \mathrm{e}^{X} + A_2 \mathrm{e}^{-X} ,$$
$$V(X) = B_1 \cosh(X) + B_2 \sinh(X) ,$$
$$V(X) = C_1 \cosh(L - X) + C_2 \sinh(L - X) ,$$

where:

$$\cosh(X) \triangleq \frac{1}{2}\left(\mathrm{e}^{X} + \mathrm{e}^{-X}\right); \ \sinh(X) \triangleq \frac{1}{2}\left(\mathrm{e}^{X} - \mathrm{e}^{-X}\right)$$

Input impedance of a semi-infinite cable:

Consider a current that is injected into the intracellular space at the origin of a *semi-infinite cable* (i.e., starts at $x = 0$ and heads off only in one direction to $x = +\infty$), with the return electrode in the extracellular space at the origin.

The *input impedance* for the semi-infinite cable is:

$$Z_0 = \frac{v_m(x=0)}{I_i(x=0)}. \qquad (7.52)$$

Input impedance of a semi-infinite cable (cont.):

For a semi-infinite cable the relative membrane potential is:

$$v_m(x) = C\mathrm{e}^{-|x|/\lambda}. \qquad (7.53)$$

Assuming $r_e \approx 0$, the intracellular axial current is:

$$I_i(x) = -\frac{1}{r_i}\frac{\partial V_m}{\partial x} = -\frac{1}{r_i}\frac{\partial v_m}{\partial x} \qquad (7.54)$$

$$= \frac{C}{r_i\lambda}\mathrm{e}^{-|x|/\lambda}. \qquad (7.55)$$

Input impedance of a semi-infinite cable (cont.):

Since $\lambda \approx (r_m/r_i)^{1/2}$ when $r_e \approx 0$:

$$I_i(x) = \frac{C}{\sqrt{r_m r_i}} \mathrm{e}^{-|x|/\lambda}, \qquad (7.56)$$

and the input impedance is:

$$Z_0 = \frac{C\mathrm{e}^{-|x|/\lambda}}{\frac{C}{\sqrt{r_m r_i}}\mathrm{e}^{-|x|/\lambda}} \qquad (7.57)$$

$$= \sqrt{r_m r_i}\,. \qquad (7.58)$$

Input impedance of a finite cable:

The input impedance Z_{in} for a *finite cable* will depend on the cable's:

- **length** (l in absolute units, or $L = l/\lambda$ in *electrotonic units*), and
- **termination impedance** (Z_L).

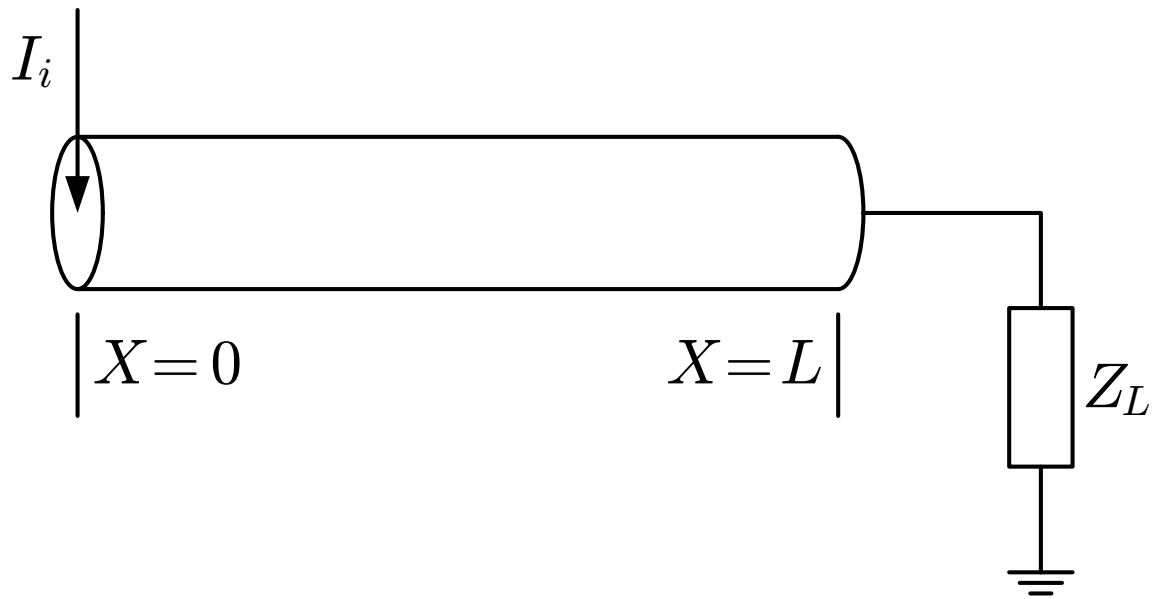

Input impedance of a finite cable:

The termination impedance is determined by the physical configuration of the end of the fiber.

Some common boundary conditions include:

- *semi-infinite cable*,
- *sealed-end*,
- *killed-end*, and
- *arbitrary-impedance*.

Input impedance of a finite cable (cont.):

- A *semi-infinite cable termination* of a finite cable corresponds to $Z_L = Z_0$. In this case, the finite cable is simply considered to be the proximal section of a semi-infinite cable.

Input impedance of a finite cable (cont.):

- A *sealed-end termination* corresponds to having a patch of membrane covering the end of the fiber, such that $Z_L \approx \infty$.
  In this case, the internal axial current must be zero at the end of the fiber, i.e., $I_i(X{=}L) = 0$.
- Using this boundary condition:

$$V(X) = V_0 \cosh(L - X) / \cosh(L) \ ,$$

$$R_{\text{in}} = R_\infty \coth(L) \ .$$

Input impedance of a finite cable (cont.):

In the case of a sealed-end termination, the shorter the finite cable, the greater the effect of the infinite termination impedance on the input impedance.

Table 7.3. Normalized Input Impedance of Finite Length Cable

L/λ	Z_{in}/Z_0
0.1	10.0
0.5	2.16
1	1.31
2	1.04
3	1.01

Input impedance of a finite cable (cont.):

- A *killed-end termination* corresponds to having a direct opening to the extracellular fluid at the end of the fiber, such that $Z_L \approx 0$. In this case, the transmembrane potential must be zero at the end of the fiber, i.e., $V_m(X{=}L) = 0$.
- Using this boundary condition:

$$V(X) = V_0 \sinh(L - X) / \sinh(L) \ ,$$

$$R_{\text{in}} = R_\infty \tanh(L) \ .$$

Input impedance of a finite cable (cont.):

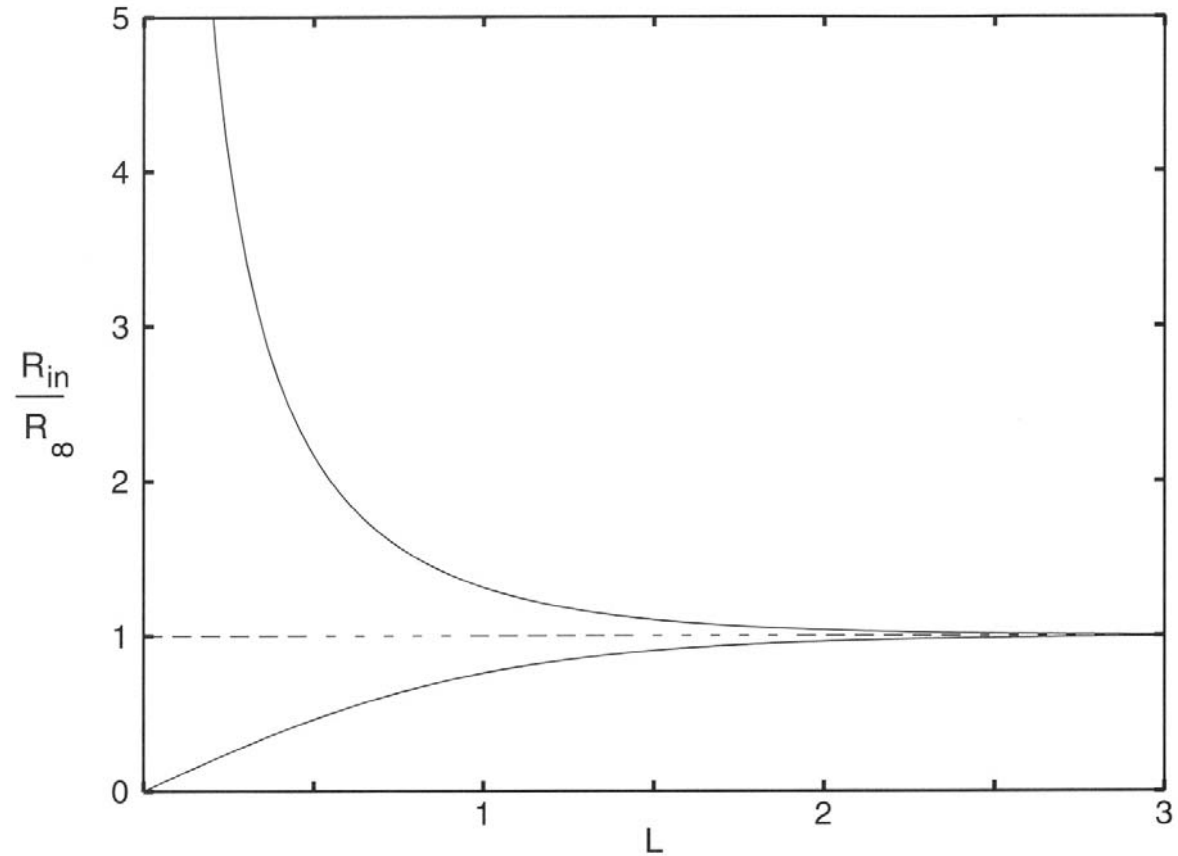

Fig. 2.5 Input Resistance of a Finite Cable Input resistance R_{in} looking into a cable of electrotonic length L toward the right terminal. The ordinate is normalized in terms of the input resistance R_{in} of a semi-infinite cylinder (Eq. 2.16). The normalized input resistance for a sealed-end boundary condition (upper curve) is always larger than R_∞, while the input resistance of a cable with killed-end boundary condition (lower curve) is always less. In the former case, the current is prevented from leaving the cable at the endpoint, while the voltage is "shorted to ground" in the latter case. For cables longer than two space constants, $R_{in} \approx R_\infty$.

(from Koch)

Input impedance of a finite cable (cont.):

- An *arbitrary-impedance* termination is often used to describe the boundary between parent and daughter branches in dendritic trees.
- Using this boundary condition:

$$V(X) = V_0 \frac{\cosh(L-X) + (R_\infty/R_L)\sinh(L-X)}{\cosh(L) + (R_\infty/R_L)\sinh(L)},$$

$$R_{\text{in}} = R_\infty \frac{R_L + R_\infty \tanh(L)}{R_\infty + R_L \tanh(L)}.$$

Steady-state response of a finite cable:

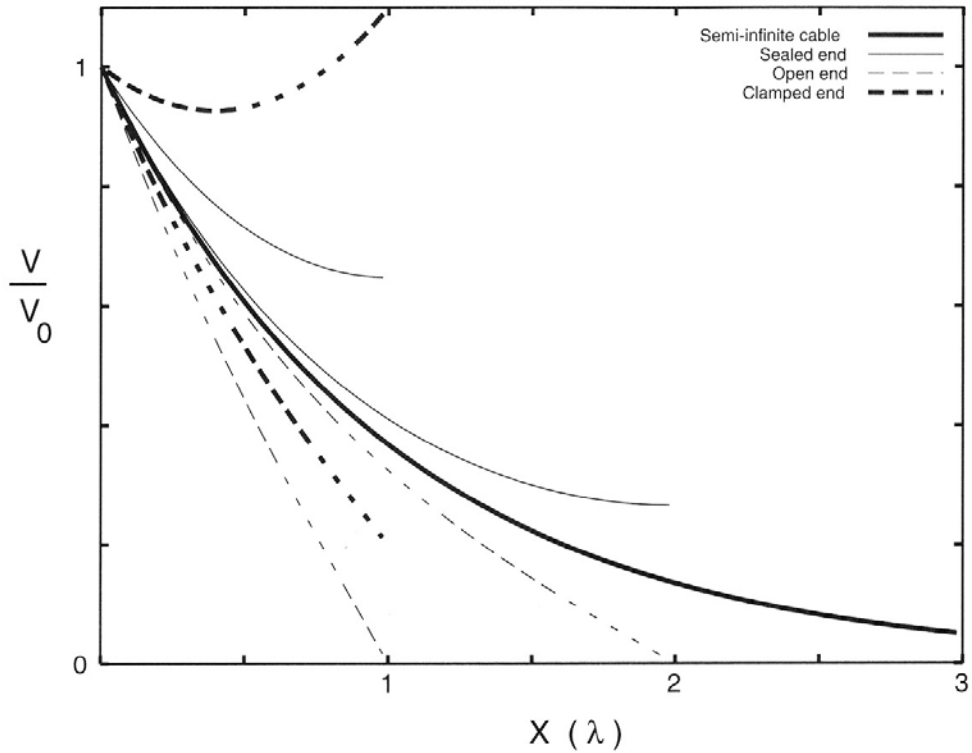

Fig. 2.4 STEADY-STATE VOLTAGE ATTENUATION Steady-state voltage attenuation in a finite piece of cable as a function of the normalized electrotonic distance $X = x/\lambda$ from the left terminal. The potential at the left terminal is always held fixed at $V = V_0$, while the normalized potential throughout the cable varies with the boundary condition at the right terminal. The bold continuous line corresponds to the voltage in a semi-infinite cable, showing a pure exponential decay. The thin continuous lines show the voltage decay for two cables that terminate in a sealed end (Eq. 2.20) at $X = 1$ or $X = 2$. This is the type of boundary condition used most commonly in simulations. The two thin dashed curves show the same two cables, but now terminating in a short circuit (killed-end boundary condition; Eq. 2.23). Note that either the spatial derivative of voltage (sealed-end) or the voltage itself (killed-end) is zero at the rightmost terminal. That the spatial voltage profile can be nonmonotonic in a passive cable is witnessed by the topmost bold dashed curve, where the voltage at $X = 1$ is clamped to 1.1 times the voltage at the origin. For the lower bold dashed curve, the voltage at the terminal is clamped to $0.2V_0$. Reprinted in modified form by permission from Rall (1989).

(from Koch)

Time-dependent response of a finite cable:

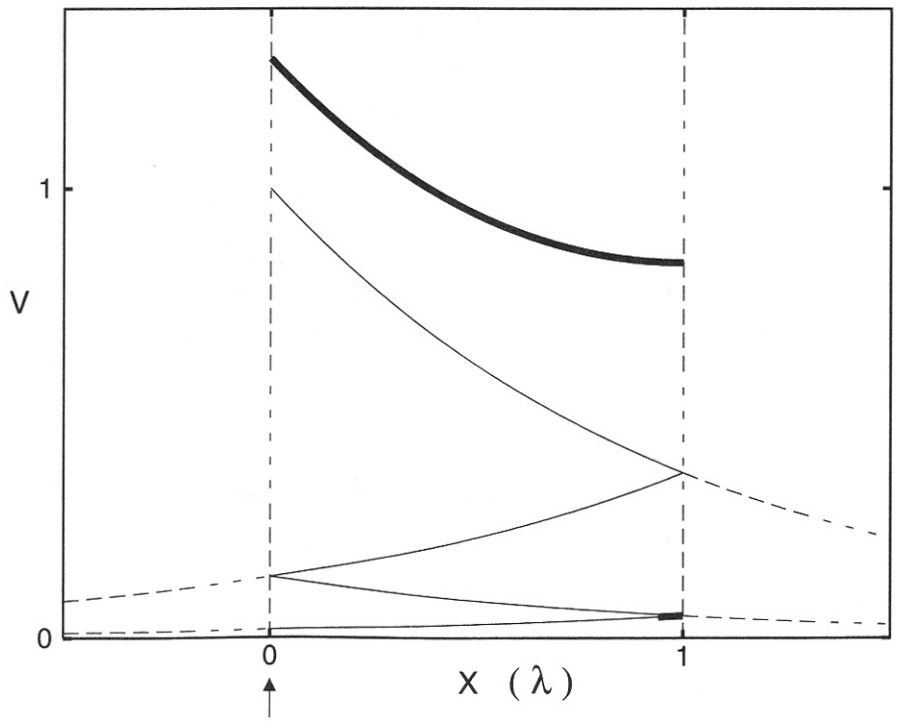

(from Koch)

Fig. 2.10 VOLTAGE RESPONSE IN A FINITE CABLE In a finite cable with sealed end boundary conditions at $X = 0$ and 1, the voltage V in response to any current input can be described as the sum (bold line) of infinitely many "reflection" terms (thin lines), each term becoming progressively smaller. This leads to the convergent series in Eq. 2.41. Here, the current is injected at $X = 0$.

Branching in passive dendritic trees:

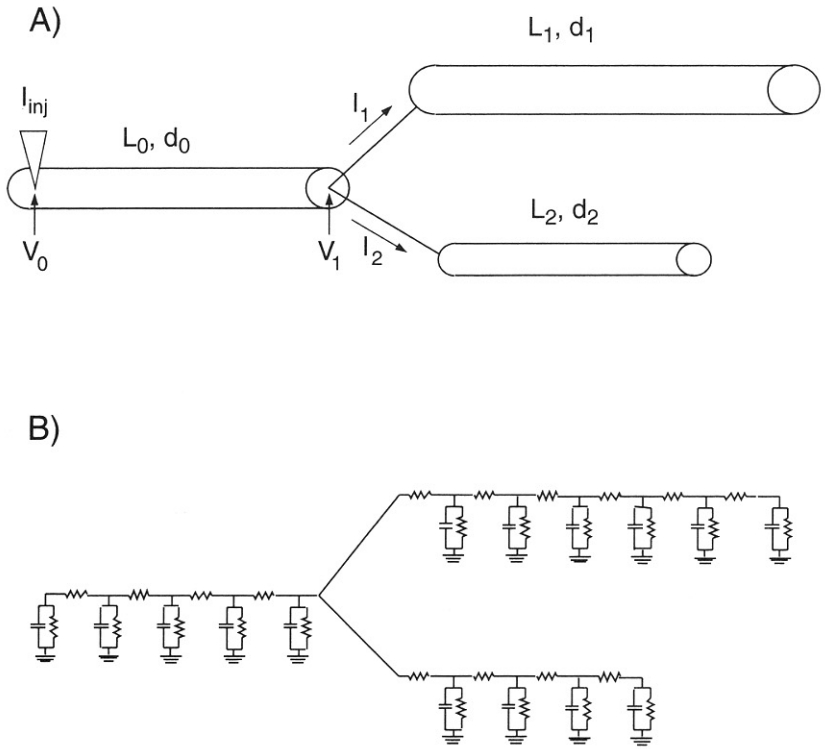

(from Koch)

Fig. 3.4 PASSIVE BRANCHING DENDRITE **(A)** Schematic drawing of a passive cylindrical dendrite, with diameter d_0 and electrotonic length $L_0 = l_0/\lambda_0$, with two daughter branches, each with its distinct diameter and electrotonic length $L_i = l_i/\lambda_i$. A simple recursive scheme exists to compute exactly the voltage in such tree structures in response to current input (Rall, 1959). All terminals are assumed to be sealed. **(B)** Compartmental-model representation of this passive dendritic tree. The voltage dynamics in this circuit approximate the solution to the cable equation of the continuous cable in **A** in the sense that the cable equation (Eq. 2.7) describes the dynamics of the membrane potential in the limit that the grid size becomes infinitely fine. For the sake of simplicity, we set V_{rest} to zero (see Fig. 2.3). Standard software packages, such as NEURON or GENESIS, automatically solve for the voltage in these circuits.

Branching in passive dendritic trees (cont.):

Assuming sealed ends on the daughter branches 1 and 2, their input impedances are:

$$R_{\mathrm{in},1} = R_{\infty,1} \coth(L_1) \ ,$$
$$R_{\mathrm{in},2} = R_{\infty,2} \coth(L_2) \ ,$$

respectively.

Thus, the parallel daughter branches are equivalent to a termination impedance given by:

$$\frac{1}{R_{L,0}} = \frac{1}{R_{\mathrm{in},1}} + \frac{1}{R_{\mathrm{in},2}}$$

Branching in passive dendritic trees (cont.):

Consequently, the input impedances of the parent branch is:

$$R_{\mathsf{in},0} = R_{\infty,0}\,\frac{R_{L,0} + R_{\infty,0}\tanh(L_0)}{R_{\infty,0} + R_{L,0}\tanh(L_0)}\,.$$

Multiple branches can be solved recursively in this manner.

Branching in passive dendritic trees (cont.):

Once the input impedance at the site of current inject is calculated, the voltage at this site can be determined via:

$$V_0 = R_{\text{in},0} I_{\text{inj}} \,,$$

and given V_0, we can compute the voltage at any point in the tree. This is achieved by calculating how much current flows into each of the daughter branches.

Branching in passive dendritic trees (cont.):

In daughter branch 1:

$$I_1(X) = \frac{V_1}{R_{\infty,1}} \frac{\sinh(L_1 - X)}{\cosh(L_1)},$$

$$\Rightarrow \quad I_1(X=0) = \frac{V_1}{R_{\text{in},1}} = V_1 G_{\text{in},1}\,.$$

Thus:

$$\begin{aligned} I_0(X=L) &= I_1(X=0) + I_2(X=0) \\ &= V_1 \left(G_{\text{in},1} + G_{\text{in},2} \right)\,. \end{aligned}$$

$\Rightarrow$ the current divides between the daughter branches according to the input conductances

Equivalent cylinder of a dendritic tree:

Assume $L_1 = L_2$ and $d_1 = d_2$

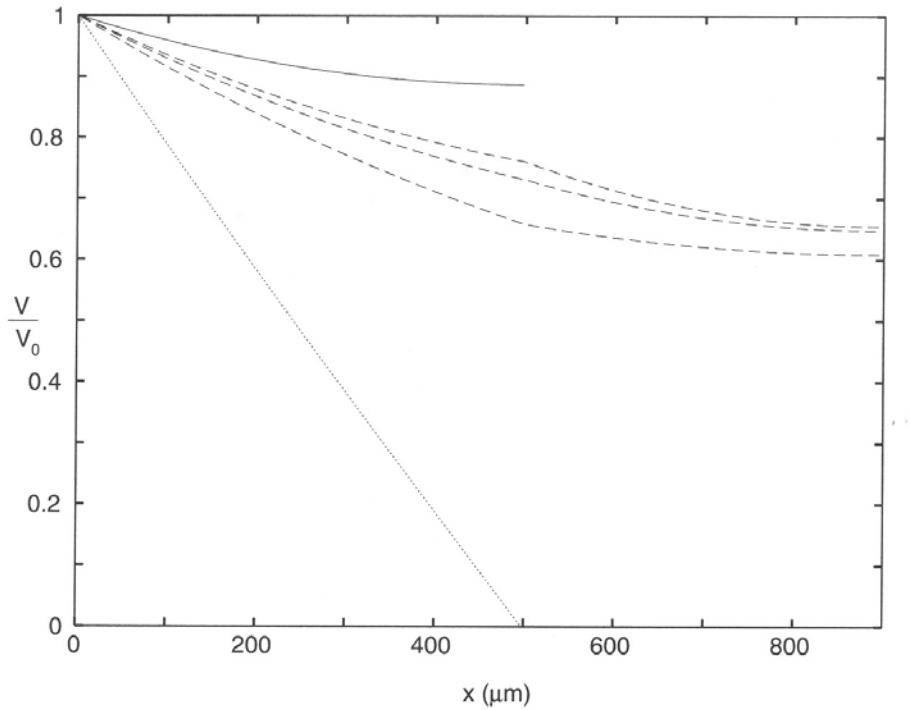

(from Koch)

Fig. 3.5 VOLTAGE DECAY ALONG A SIMPLE DENDRITIC TREE Steady-state voltage decay along the tree shown in Fig. 3.4A, assuming that the two daughter branches are identical, with $d_1 = d_2$ and $L_1 = L_2 = 0.5$. The three dashed curves correspond to (1) $d_0 = 2d_1$, (2) $d_0^{3/2} = 2d_1^{3/2}$, and (3) $d_0 = d_1$. For the dotted curve, the potential at the right-hand terminal of the main branch is set to zero (short circuit). For the upper, continuous curve, the membrane is sealed. At the branchpoint $x = 500\,\mu$m, the voltage profile has a discontinuous derivative for $d_0 = 2d_1$ and for $d_0 = d_1$. If the input resistance of the parent at this point is matched to that of the daughter branches (as is the case for the second condition, $d_0^{3/2} = 2d_1^{3/2}$), the voltage decay across the cables can be described by a single, simple expression. This trick is exploited by Rall in his concept of the *equivalent tree*.

Equivalent cylinder of a dendritic tree (cont.):

In the case of ${d_0}^{3/2} = 2{d_1}^{3/2}$, all derivatives of the voltage profile are continuous $\Rightarrow$ the voltage decay can be described by a single expression.

Why?

$$\frac{1}{R_{L,0}} = \frac{1}{R_{\infty,1}\coth(L_1)} + \frac{1}{R_{\infty,1}\coth(L_1)}$$

$$\Rightarrow \qquad R_{L,0} = \frac{R_{\infty,1}\coth(L_1)}{2}\,.$$

Equivalent cylinder of a dendritic tree (cont.):

For a semi-infinite cable:

$$R_{\infty,0} = \sqrt{\frac{R_m R_i}{\pi^2}} \cdot \frac{2}{d_0^{3/2}}$$

If ${d_0}^{3/2} = 2{d_1}^{3/2}$:

$$R_{\infty,0} = \sqrt{\frac{R_m R_i}{\pi^2}} \cdot \frac{1}{d_1^{3/2}} = \frac{R_{\infty,1}}{2}$$

$\Rightarrow$ Input impedances are matched

Equivalent cylinder of a dendritic tree (cont.):

Consequently:

$$R_{L,0} = R_{\infty,0} \coth(L_1)$$

and:

$$V(X) = V_0 \frac{\cosh(L_0 + L_1 - X)}{\cosh(L_0 + L_1)} .$$

$\Rightarrow$ A parent branch of length L_0 with two identical impedance-matched daughter branches of length L_1 is equivalent to a single cylinder of length $L_0 + L_1$.

Equivalent cylinder of a dendritic tree (cont.):

Rall showed that the entire dendritic tree can be collapsed into a single equivalent cylinder if:

1. R_m and R_i are the same in all branches,
2. all terminals end in the same boundary condition,
3. all terminal branches end at the same electrotonic distance $L = \Sigma_i \, L_i$, and
4. ${d_0}^{3/2} = {d_1}^{3/2} + {d_2}^{3/2}$ at every branch point.

Assumptions 1 & 2 are reasonable, but 3 & 4 are only met in a few remarkable neuron types.

Compartmental modeling:

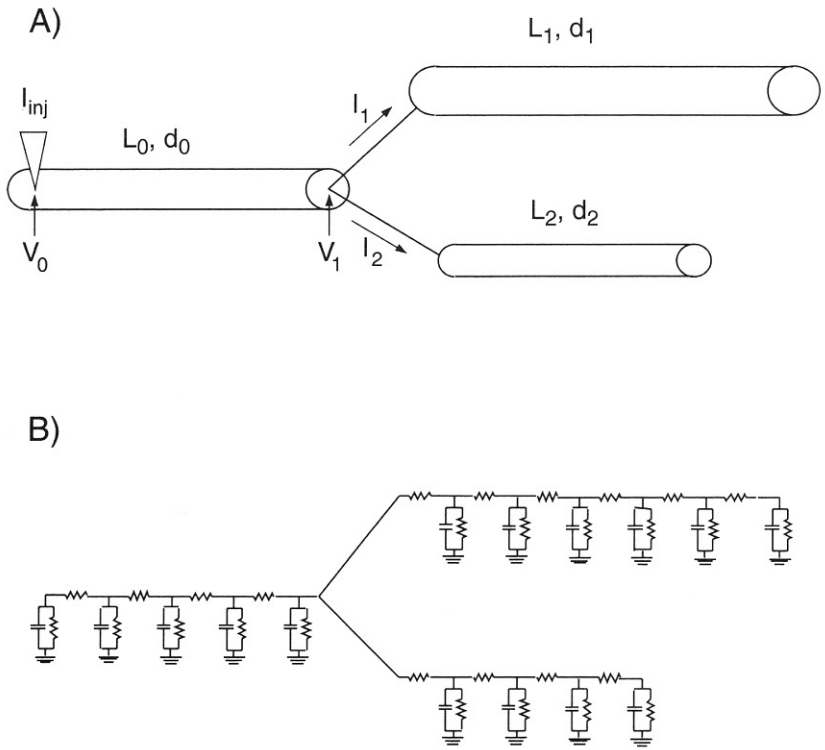

(from Koch)

Fig. 3.4 PASSIVE BRANCHING DENDRITE **(A)** Schematic drawing of a passive cylindrical dendrite, with diameter d_0 and electrotonic length $L_0 = l_0/\lambda_0$, with two daughter branches, each with its distinct diameter and electrotonic length $L_i = l_i/\lambda_i$. A simple recursive scheme exists to compute exactly the voltage in such tree structures in response to current input (Rall, 1959). All terminals are assumed to be sealed. **(B)** Compartmental-model representation of this passive dendritic tree. The voltage dynamics in this circuit approximate the solution to the cable equation of the continuous cable in **A** in the sense that the cable equation (Eq. 2.7) describes the dynamics of the membrane potential in the limit that the grid size becomes infinitely fine. For the sake of simplicity, we set V_{rest} to zero (see Fig. 2.3). Standard software packages, such as NEURON or GENESIS, automatically solve for the voltage in these circuits.